Journal of Materials Chemistry C

ROYAL SOCIETY OF CHEMISTRY

COMMUNICATION

View Article Online
View Journal | View Issue

Cite this: J. Mater. Chem. C, 2021, 9, 16192

Received 28th July 2021,
Accepted 24th September 2021

DOI: 10.1039/d1tc03506a

rsc.li/materials-c

Single-molecule conductance variations of up to four orders of magnitude *via* contacting electrodes with different anchoring sites†‡

Zhiyu Zhu,[a] Hang Qu,[a] Yaorong Chen,[a] Chengyang Zhang,[a] Ruihao Li,[a] Yi Zhao,[a] Yu Zhou,[a] Zhixin Chen,*[ab] Junyang Liu,[a] Zongyuan Xiao*[a] and Wenjing Hong*[a]

Control of conductance through a single molecule *via* alternating anchoring points provides a unique perspective to design single-molecule electronic devices. A high conductance difference among different states is essential for a single-molecule electronic device, which is challenging due to restriction of the structural changes in single-molecule junctions. Here, tetraphenylethylene derivatives with multiple anchoring sites are designed and synthesized to investigate single-molecule conductance using the scanning tunneling microscope break junction (STM-BJ) technique. In the break-junction cycle process, connection conformations with different anchor sites have been achieved reversibly to switch single-molecule conductance using the STM-BJ technique. Through mechanical control, these multi-anchored single-molecule junctions can achieve up to three conductance switching cycles, and the variation in conductance reaches up to four orders of magnitude. Theoretical calculations reveal that the conductance change originates from the different connecting sites and the different anchored configurations of single-molecule junctions provide a significantly different transmission. Our findings provide a reliable strategy to manipulate the mechanical switching and shed light on investigating the intrinsic charge transport of multi-anchored molecules.

Introduction

Utilizing molecules in electronics devices provides an essential step in the roadmap for the miniaturization and functionalization of electronic components.[1–7] To improve the signal-to-noise ratio of electronic devices during operation, high conductance differences among the different states are essential for single-molecule devices.[8–12] Molecular isomerization, as a common and effective method for designing molecular conductance switches, is widely utilized to implement high conductance differences primarily within 2 orders of magnitude of switching factors.[13–22] However, this strategy requires specific conditions such as pH regulation[13,14,21] or external field modulation[15–17,22] to activate the molecules, while a high switching factor is challenging since the electronic structures in different states are similar.[23–25] The mechanical modulation of particular binding sites between the molecule and the electrodes to vary the conductance provides a better opportunity to achieve more conductance states and a significantly higher switching factor by rational design of molecular structures.[26–28]

With this strategy, different anchoring sites between the molecule and the electrodes could be well controlled *via* mechanical tuning to switch various junction states.[29] The control of conductance by alternating anchoring sites has recently been reported, such as bisthioanisole substituted 1,2-disilaacenaphthenes[30] and pyridinium in the middle of the molecular skeleton.[31] However, switching factors with only two changeable conductance states are still relatively low. To maximize the switching factor in single-molecule junctions, we designed a new type of molecule to achieve up to tri-stable conductance switching as a result of different anchoring sites providing various conduction pathways, in which a four orders of magnitude change in switching factor has been achieved.

In this work, we designed and investigated the charge transport properties of two types of tetraphenylethylene derivatives. Through molecular engineering, multiple anchoring sites are introduced in the molecular chain to construct single-molecule junctions using the scanning tunneling microscopy break junction (STM-BJ) technique to switch conductance as a molecular mechanical switch,[32–36] as shown in Scheme 1. Moreover, the value of conductance shifts in three states, and the highest switching factor is more than four orders of

[a] State Key Laboratory of Physical Chemistry of Solid Surfaces, iChEM, College of Chemistry and Chemical Engineering, Xiamen University, Xiamen 361005, China. E-mail: xiaozy@xmu.edu.cn, whong@xmu.edu.cn
[b] Department of Materials, University of Oxford, Parks Road, Oxford OX1 3PH, UK. E-mail: zhixin.chen@materials.ox.ac.uk

† Dedicated to Professor Kees Hummelen on the occasion of his retirement.

‡ Electronic supplementary information (ESI) available. See DOI: 10.1039/d1tc03506a

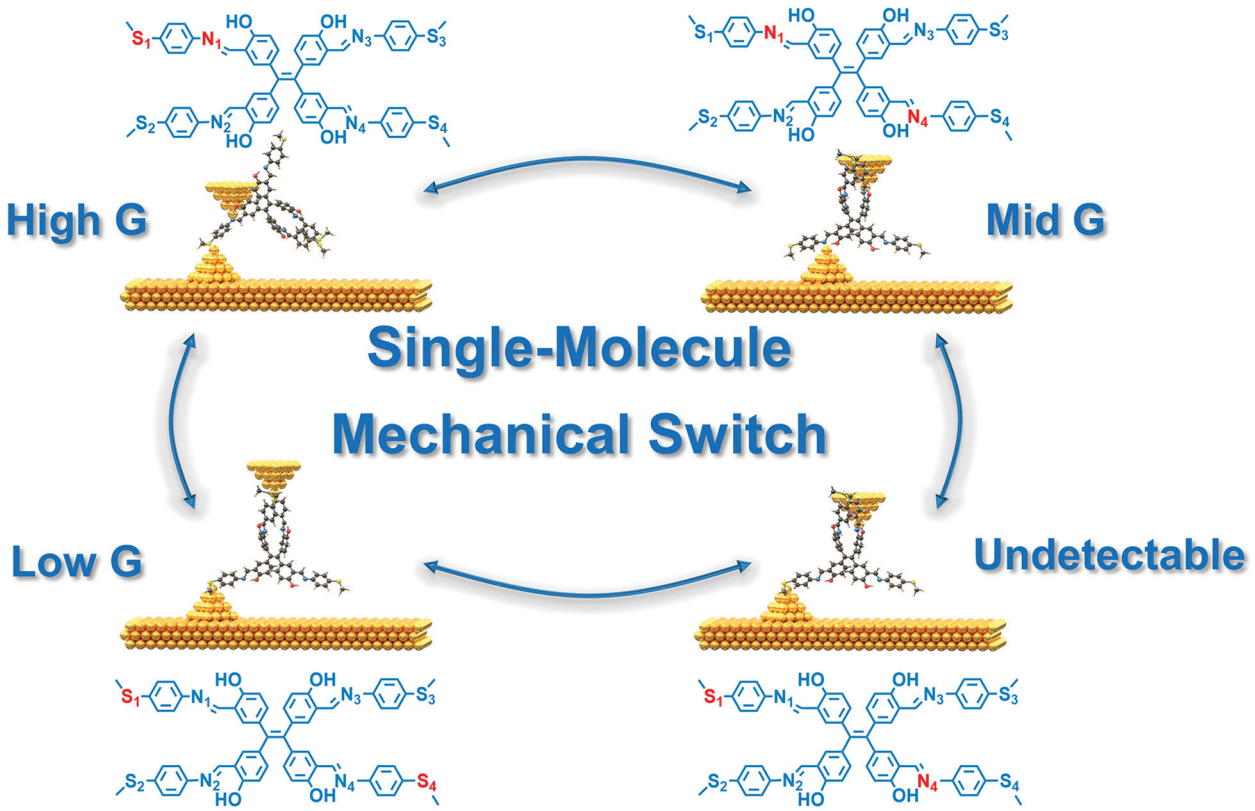

Scheme 1 Schematic of the single-molecule junction and mechanical molecular switch based on multiple anchoring sites. The spatial structures of the molecules are optimized structures from DFT calculations.

magnitude larger, which is ten times higher than the recently reported highest value.[31] The compression–elongation experiments demonstrated the reversibility of the single-molecule switches. The flicker noise analysis combined with DFT theoretical calculations elucidates that every conductance for each molecular structure corresponds to through-bond transport mechanisms. Our results provide an in-depth insight towards the study of multi-anchoring molecules and expand the avenue for designing single-molecule mechanical switches.

Results and discussion

STM-BJ conductance measurement

These two tetraphenylethylene derivatives, as shown in Fig. 1a, were measured using the STM-BJ technique. Typical individual conductance traces are randomly selected from break junction cycles, as shown in Fig. 1b–e. On comparing the traces in the same break-junction cycle, for both **TPE-m-OH** and **TPE-p**, the closing traces exhibit a trend of increasing conductivity as the electrode nanogap decreases, while the opening traces are the opposite. In every opening and closing cycle, the targeted molecules present multiple plateaus, indicating the construction of molecular junctions, which is related to the distance between electrodes and shows great potential for mechanical switches. **TPE-m-OH** shows three obvious plateaus at about $10^{-2.07}$ G_0, $10^{-3.88}$ G_0 and $10^{-5.54}$ G_0, where G_0 means quantum conductance and equals 77.5 μS.[37] For **TPE-p**, two prominent plateaus are observed located at about $10^{-2.0}$ G_0 and $10^{-6.1}$ G_0, respectively. These results show the potential for being utilized as mechanical molecular switches since their high switching factors (3.5 and 4 orders of magnitude higher, respectively) and the conductance could switch between two or three states, which presents remarkable superiority over other molecular systems.

In the one-dimensional (1D) conductance diagrams, peaks are exhibited for **TPE-m-OH** and **TPE-p** (Fig. 1f and g). The three conductance peaks of the **TPE-m-OH** junction are determined at $10^{-2.07}$ G_0, $10^{-3.88}$ G_0 and $10^{-5.54}$ G_0 by Gaussian fitting, while for **TPE-p**, two distinct conductance peaks are observed, where the low conductance is $10^{-6.2}$ G_0, and the high conductance is $10^{-2.04}$ G_0, which is consistent with the aforementioned individual conductance trace results. Correlation analysis and control experiments confirm that the signals derive from the same molecule (see more details in Fig. S4 in the ESI‡).

To further explore the origin of the mechanical switching behavior, two-dimensional (2D) histograms are constructed (more than 3000 stretching traces of the targeted molecules without data selection) to elucidate the relationship between conductance and displacement (Fig. 1h and i). The clear plateaus illustrate the successful construction of single-molecule junctions. Considering the Au–Au snap–back distance (0.5 nm),[38] the length of junctions for **TPE-m-OH** are calibrated to be ~0.62 nm (high conductance), ~1.2 nm (medium conductance) and ~1.95 nm (low conductance). As for **TPE-p**, the

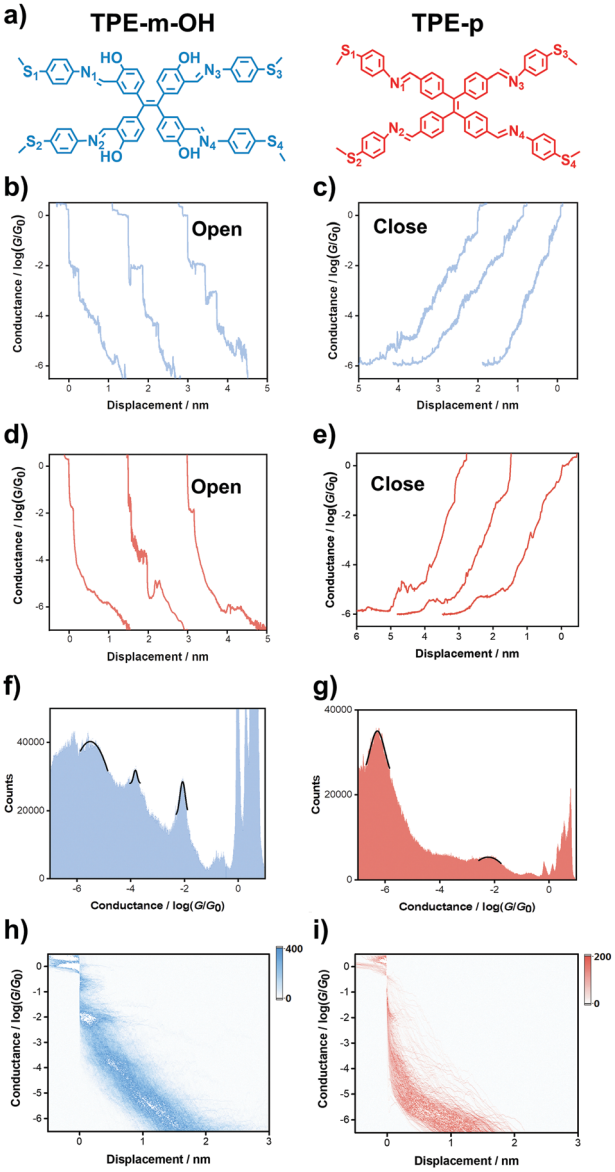

Fig. 1 (a) Molecular structures of **TPE-m-OH** (blue), **TPE-p** (red). (b–e) Typical individual conductance distance traces in the opening and closing process for **TPE-m-OH** (blue) and **TPE-p** (red), respectively. (f and g) The one-dimensional (1D) conductance histograms of **TPE-m-OH** (blue) and **TPE-p** (red). (h and i) Two-dimensional (2D) conductance histograms *versus* relative displacement for **TPE-m-OH** (blue) and **TPE-p** (red).

length of the junctions is determined to be around ~0.6 nm for high conductance and ~2.48 nm for low conductance, which illustrates that the variations in conductance result from the different anchoring sites (see Fig. S2 in the ESI‡ for more details). The distinguished density clouds demonstrate the robustness of the switching process, indicating these two types of molecule could serve as single-molecule mechanical switches.

To further investigate the reversibility of the single-molecule mechanical switches, compression–elongation experiments were carried out. The junctions were elongated at the position where the conductance can be captured according to the

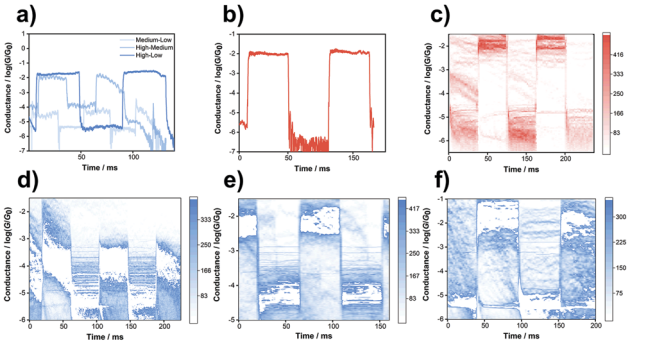

Fig. 2 (a and b) Sample traces of **TPE-m-OH** and **TPE-p** for conductance changing with the compression–elongation of piezo. (c) A 2D histogram constructed from selected traces for **TPE-p**. (d–f) A 2D histogram was constructed from selected traces for **TPE-m-OH** for conductance switching between (d) medium and low conductance, (e) high and medium conductance, and (f) high and low conductance.

conductance mentioned above. Then, a square wave was applied to the piezo to adjust the distance between the tip and the substrate. In this condition, the structures of the molecular junction were repeatedly elongated or compressed in correlation with the piezo movements to modulate the conductance by mechanical control. The tip–substrate distance was modulated by the piezo applied with the square wave, and for **TPE-m-OH** the tip–substrate distance was modulated by 0.58 nm, 0.75 nm and 1.2 nm for the switch between high–medium, medium–low and high–low conductance respectively, while for **TPE-p**, the tip–substrate distance was modulated by 1.9 nm. The frequency of the square wave remains constant (500 Hz), and the continuous and reverse regulation of switching between the two states are correlated with the wave amplitude, which is presented in Fig. 2. Hundreds of traces were collected to construct a 2D histogram, as shown in Fig. 2c–f. The conductance of **TPE-m-OH** and **TPE-p** switching among the high, medium and low conductance states is successfully observed, validating the reproducibility of the switching process for an individual junction. For the switch between the medium conductance state and the low conductance state of **TPE-m-OH**, the conductance always drops down to a conductance level that is below the low conductance state after the transition point, and then jumps up to the low conductance state, and *vice versa*, which might be attributed to the transition through an undetectable state during the transition process (S_1–N_4 anchoring sites, see more details in Fig. S5f in the ESI‡). Additionally, the highest switching factor (more than four orders of magnitude) was obtained in Fig. 2c, and its performance is improved approximately by one order of magnitude compared with previous work.[28,29]

According to the principle of the break-junction process, before the molecule forms a molecular junction, one of the terminal groups is adsorbed on the surface of the electrode. When the gold tip is moving in and out of contact with the gold substrates, it anchors with another terminal group to form a molecular junction. Therefore, the low-G state and the mid-G state could not transform mutually, which further indicates the

existence of an undetectable state during the transition process between the medium conductance state and the low conductance state. The possible mechanism of the transitions between different conductance states is shown in Fig. S7 in the ESI.‡ However, during one break-junction cycle, the tip could connect with any anchoring sites along with the movement, hence the correlation between any of the two states of conductance should still be positive, as the 2D correlation histograms show in Fig. S4 in the ESI.‡

Flicker noise analysis

To further investigate the charge transport mechanism through junctions with different anchoring sites, flicker noise analysis of both target molecules was performed.[39–42] The molecular junctions are suspended for about 150 ms to extract signals for subsequent analysis. Typical traces are shown in Fig. S3 (ESI‡). Generally, a higher value of n is obtained due to the stronger correlation between noise and conductance, corresponding to through-space charge transport. In contrast, a lower n indicates the charge transport is dominated by through-bond charge transport.[41,43]

The 2D histograms of flicker noise power *versus* average conductance for **TPE-m-OH** and **TPE-p** are shown in Fig. 3a–e, respectively (2D histograms normalized for noise power *versus* conductance are presented in Fig. S3, ESI‡). The noise power of **TPE-m-OH** scaled as $G^{1.2}$, $G^{1.3}$ and $G^{1.4}$ for high, medium and low conductance, respectively, indicating that the charge transport through the junction is dominated by through-bond transport. Moreover, the noise power of **TPE-p**, which is scaled as $G^{1.2}$ for both the high conductance and the low conductance states, shows a similar transport behavior to that of **TPE-p**. These results explain that all of the probable connecting patterns exhibit a similar transport mechanism. In addition, according to previous research, single-stacking junctions show stronger through-space transport and the noise power tends to scale as $G^{2.0}$.[44] The noise power of both molecules are close to $G^{1.0}$, which demonstrates that the multiple conductance does not derive from the stacking configuration.

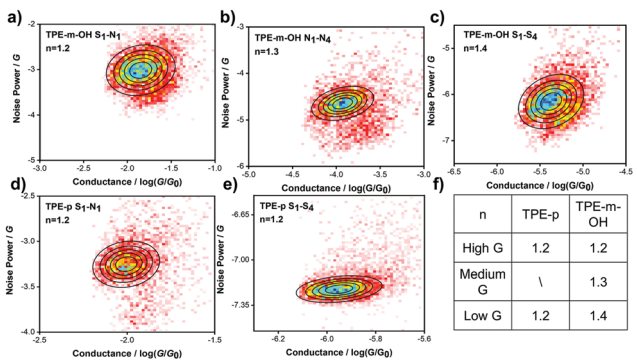

f)

n	TPE-p	TPE-m-OH
High G	1.2	1.2
Medium G	\	1.3
Low G	1.2	1.4

Fig. 3 (a–c) The noise power *versus* averaged conductance for **TPE-m-OH** in high (a), medium (b) and low conductance plateaus (c). (d and e) The noise power *versus* averaged conductance for **TPE-p** in high (d) and low conductance plateaus (e). (f) Statistics for the values of the normalized parameter n under different conductance values.

Theoretical calculations

To further understand the charge transport through the single-molecule junctions with different anchoring sites, theoretical calculations were carried out, and all possible connected junctions are counted and optimized (see Fig. S4 in the ESI‡ for more details). The numbering of atoms is as shown in Fig. 1a. Among them, the distance for **TPE-m-OH** (S_1–N_1 anchoring sites of 0.6 nm, N_1–N_4 anchoring sites of 1.2 nm and S_1–S_4 anchoring sites of 1.9 nm) and the distance for **TPE-p** (S_1–N_1 anchoring sites of 0.6 nm and S_1–S_4 anchoring sites of 2.5 nm) are consistent with the length of the junctions determined by the experimental results. The results of the binding energy calculations reveal the strong interaction of Au–N bonds, validating that the medium conductance from the N_1–N_4 anchoring conformation is energy allowed (see more details in Fig. S6 and S8, ESI‡). The transmission spectra are calculated to illustrate the relationship between conductance and anchoring sites, as shown in Fig. 4a and b. It is found that the S_1–S_4 anchoring sites have the lowest transmission coefficient, while the transmission coefficient of the S_1–N_1 anchoring sites is the highest in both molecules.[45,46]

The transmission pathway calculation is adopted to reveal the charge transport mechanism through the molecules exhibited in Fig. 4c–e.[47,48] For every possible anchoring mode in **TPE-m-OH** and **TPE-p**, the transmission pathways show the current majorly flows between neighboring atoms through chemical bonds (see more details in Fig. S6 in, ESI‡), indicating the through-bond transport mechanism. Those theoretical calculation results fit well with the experimental consequences mentioned in the previous discussion, indicating the multiple conductance originates from the various anchoring sites, and all of these possible anchoring methods conform to the through-bond mechanism.

In our previous study,[43] it has been demonstrated that hydroxy substituents whose orientations were fixed by intramolecular hydrogen bonds with imide groups could

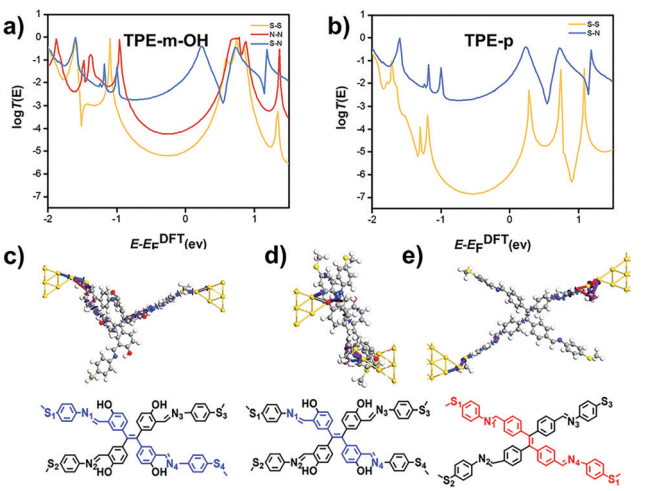

Fig. 4 (a and b) Calculated transmission spectra for **TPE-m-OH** (a) and **TPE-p** (b) with different anchoring sites. (c–e) The transmission path for S_1–S_4 (c), the N_1–N_4 anchoring site of **TPE-m-OH** (d), and the S_1–S_4 anchoring site of **TPE-p** (e).

significantly suppress the destructive quantum interference raised by *meta*-connected benzene, for which the *meta*-connected benzene could show a similar charge transport capability to that of *para*-connected benzene. Additionally, the hydroxy group is a strong electron-donating group on pi-systems, which could increase electron density on the benzene ring, and further increase the anchoring capability of adjacent nitrogen atoms, for which tri-stable conductance switching could be achieved. Besides, the intramolecular hydrogen bonds make the molecule **TPE-m-OH** more planar, making it easier to achieve intramolecular stacking as shown in Scheme 1. The intramolecular stacking does not contribute to through-space transport, which has been demonstrated by transmission pathway calculations. However, this stacking in some degree increases the electron cloud density on the benzene rings, which may also further increase the charge transport capability of the benzene ring and increase the anchoring capability of the atoms.

Conclusions

In conclusion, we designed, synthesized, and investigated the charge transport through the single-molecule junctions of two tetraphenylethylene derivatives **TPE-m-OH** and **TPE-p**, using the STM-BJ technique. The molecules are designed and synthesized with multiple anchoring sites, which exhibit two and three variable conductance values, respectively. The switching factor of **TPE-m-OH** is 3.5, while that of **TPE-p** rises by four orders of magnitude, which is more than one order of magnitude larger than the highest value reported in previous studies. The flicker noise analysis combined with theoretical calculations confirms this viewpoint and reveals that a through-bond mechanism dominates the charge transport through different states. The combined calculation and the experimental investigations reveal that the origin of the different conductance values comes from the different connections between various anchoring sites and the electrodes. Our work provides a novel and constructive perspective for designing next-generation electronic components with multiple states and significant switching factors.

Experimental section

Materials

TPE-m-OH and **TPE-p** were designed and synthesized by imine condensation. See more details in the ESI.‡

Scanning tunneling microscopy break junction measurements

The single-molecule conductance was acquired using a lab-built STM-BJ setup under ambient environmental conditions and at room temperature. Before the conductance measurements, a calibration was conducted in a pure solvent to acquire accurate conductance information *versus* distance. See more details in the ESI.‡ Then all single-molecule conductance values were measured in a solution containing 0.1 mM of the targeted molecules in 1,2,4-trichlorobenzene (TCB). The molecular junctions were constructed by repeatedly moving the tips in and out of contact with the gold substrates, which was precisely regulated using a stepper motor and a piezo stack. A fixed bias voltage of 100 mV was applied between the tips and substrates. The conductance *versus* displacement traces were collected in every opening (tip retracting) and closing (tip approaching) cycle for further analysis.

Compression–elongation experiments

When the conductance reached the required range, the tip was held over the electrodes for about 200 ms, and the triangular wave was applied to the piezo to elongate and compress the distance between electrodes to match the length of the molecules. The reversible and reproducible switching between the two different states reveals the excellent mechanical switching performance.

Flicker noise analysis on molecular junctions

A flicker noise analysis of the molecular junctions was conducted based on previous studies. According to the previous research, the scaling factor n, which could be obtained by dividing the average conductance into the noise power G, is usually used to quantize the correlation. About 3000 traces without data selection are collected during the suspending period, and the fast Fourier transform is used to analyze the noise spectra by the integration from 100 to 1000 Hz for the plot of the noise power *versus* the average conductance, which elucidates the pattern of coupling.

Theoretical calculations

All of the molecular structures in this work are optimized using the B3LYP method and 6-31g* basis sets *via* Gaussian 16 software. The configuration of the devices was optimized using the ATK software package. The energy-dependent transmission coefficient $T(E)$ is calculated using DFT combined with the non-equilibrium Green's function (NEGF) formalism using the ATK software package.[14,49] See the ESI‡ for more details.

Conflicts of interest

There are no conflicts to declare.

Acknowledgements

This work was supported by the Open Fund of Guangdong Provincial Key Laboratory of Luminescence from Molecular Aggregates (2019B030301003), the National Key R&D Program of China (2017YFA0204902), the National Natural Science Foundation of China (No. 21673195, 21722305, 21703188, U1705254), the China Postdoctoral Science Foundation (No. 2017M622060) and the Young Thousand Talent Project of China.

Notes and references

1 M. Ratner, *Nat. Nanotechnol.*, 2013, **8**, 378–381.

2 E. Lörtscher, *Nat. Nanotechnol.*, 2013, **8**, 381–384.
3 M. Koole, J. M. Thijssen, H. Valkenier, J. C. Hummelen and H. S. J. van der Zant, *Nano Lett.*, 2015, **15**, 5569–5573.
4 G. K. Ramachandran, *Science*, 2003, **300**, 1413–1416.
5 H. Song, M. A. Reed and T. Lee, *Adv. Mater.*, 2011, **23**, 1583–1608.
6 F. Meng, Y.-M. Hervault, Q. Shao, B. Hu, L. Norel, S. Rigaut and X. Chen, *Nat. Commun.*, 2014, **5**, 3023.
7 S. J. van der Molen, *Nat. Nanotechnol.*, 2013, **8**, 622–623.
8 C. Jia, J. Wang, C. Yao, Y. Cao, Y. Zhong, Z. Liu, Z. Liu and X. Guo, *Angew. Chem., Int. Ed.*, 2013, **52**, 8666–8670.
9 S. Kumar, J. T. van Herpt, R. Y. N. Gengler, B. L. Feringa, P. Rudolf and R. C. Chiechi, *J. Am. Chem. Soc.*, 2016, **138**, 12519–12526.
10 J. Li, P. Shen, S. Zhen, C. Tang, Y. Ye, D. Zhou, W. Hong, Z. Zhao and B. Z. Tang, *Nat. Commun.*, 2021, **12**, 167.
11 D. Stefani, M. Perrin, C. Gutiérrez-Cerón, A. C. Aragonès, J. Labra-Muñoz, R. D. C. Carrasco, Y. Matsushita, Z. Futera, J. Labuta, T. H. Ngo, K. Ariga, I. Díez-Pérez, H. S. J. Van Der Zant, D. Dulić and J. P. Hill, *ChemistrySelect*, 2018, **3**, 6473–6478.
12 S. Cai, W. Deng, F. Huang, L. Chen, C. Tang, W. He, S. Long, R. Li, Z. Tan, J. Liu, J. Shi, Z. Liu, Z. Xiao, D. Zhang and W. Hong, *Angew. Chem., Int. Ed.*, 2019, **58**, 3829–3833.
13 L. Herrer, S. Martín, A. González-Orive, D. C. Milan, A. Vezzoli, R. J. Nichols, J. L. Serrano and P. Cea, *J. Mater. Chem. C*, 2021, **9**, 2882–2889.
14 Z. Li, M. Smeu, S. Afsari, Y. Xing, M. A. Ratner and E. Borguet, *Angew. Chem., Int. Ed.*, 2014, **53**, 1098–1102.
15 D. Roldan, V. Kaliginedi, S. Cobo, V. Kolivoska, C. Bucher, W. Hong, G. Royal and T. Wandlowski, *J. Am. Chem. Soc.*, 2013, **135**, 5974–5977.
16 C. Jia, A. Migliore, N. Xin, S. Huang, J. Wang, Q. Yang, S. Wang, H. Chen, D. Wang, B. Feng, Z. Liu, G. Zhang, D.-H. Qu, H. Tian, M. A. Ratner, H. Q. Xu, A. Nitzan and X. Guo, *Science*, 2016, **352**, 1443–1445.
17 X. Huang and T. Li, *J. Mater. Chem. C*, 2020, **8**, 821–848.
18 E. Leary, C. Roche, H.-W. Jiang, I. Grace, M. T. González, G. Rubio-Bollinger, C. Romero-Muñiz, Y. Xiong, Q. Al-Galiby, M. Noori, M. A. Lebedeva, K. Porfyrakis, N. Agrait, A. Hodgson, S. J. Higgins, C. J. Lambert, H. L. Anderson and R. J. Nichols, *J. Am. Chem. Soc.*, 2018, **140**, 710–718.
19 X. Yin, J. Z. Low, K. J. Fallon, D. W. Paley and L. M. Campos, *Chem. Sci.*, 2019, **10**, 10733–10739.
20 T. A. Su, H. Li, M. L. Steigerwald, L. Venkataraman and C. Nuckolls, *Nat. Chem.*, 2015, **7**, 215–220.
21 R. J. Brooke, D. S. Szumski, A. Vezzoli, S. J. Higgins, R. J. Nichols and W. Schwarzacher, *Nano Lett.*, 2018, **18**, 1317–1322.
22 F. Meng, Y.-M. Hervault, L. Norel, K. Costuas, C. Van Dyck, V. Geskin, J. Cornil, H. H. Hng, S. Rigaut and X. Chen, *Chem. Sci.*, 2012, **3**, 3113.
23 M. Taniguchi, M. Tsutsui, K. Yokota and T. Kawai, *Chem. Sci.*, 2010, **1**, 247.
24 J. L. Zhang, J. Q. Zhong, J. D. Lin, W. P. Hu, K. Wu, G. Q. Xu, A. T. S. Wee and W. Chen, *Chem. Soc. Rev.*, 2015, **44**, 2998–3022.
25 I. Franco, C. B. George, G. C. Solomon, G. C. Schatz and M. A. Ratner, *J. Am. Chem. Soc.*, 2011, **133**, 2242–2249.
26 T. A. Su, M. Neupane, M. L. Steigerwald, L. Venkataraman and C. Nuckolls, *Nat. Rev. Mater.*, 2016, **1**, 16002.
27 E. Leary, A. La Rosa, M. T. González, G. Rubio-Bollinger, N. Agraït and N. Martín, *Chem. Soc. Rev.*, 2015, **44**, 920–942.
28 M. Kiguchi, T. Ohto, S. Fujii, K. Sugiyasu, S. Nakajima, M. Takeuchi and H. Nakamura, *J. Am. Chem. Soc.*, 2014, **136**, 7327–7332.
29 J. S. Meisner, M. Kamenetska, M. Krikorian, M. L. Steigerwald, L. Venkataraman and C. Nuckolls, *Nano Lett.*, 2011, **11**, 1575–1579.
30 N. T. Kim, H. Li, L. Venkataraman and J. L. Leighton, *J. Am. Chem. Soc.*, 2016, **138**, 11505–11508.
31 C. Tang, J. Zheng, Y. Ye, J. Liu, L. Chen, Z. Yan, Z. Chen, L. Chen, X. Huang, J. Bai, Z. Chen, J. Shi, H. Xia and W. Hong, *iScience*, 2020, **23**, 100770.
32 V. Kaliginedi, P. Moreno-García, H. Valkenier, W. Hong, V. M. García-Suárez, P. Buiter, J. L. H. Otten, J. C. Hummelen, C. J. Lambert and T. Wandlowski, *J. Am. Chem. Soc.*, 2012, **134**, 5262–5275.
33 Y. Komoto, S. Fujii, M. Iwane and M. Kiguchi, *J. Mater. Chem. C*, 2016, **4**, 8842–8858.
34 B. Xu, *Science*, 2003, **301**, 1221–1223.
35 A. C. Aragonès, N. L. Haworth, N. Darwish, S. Ciampi, N. J. Bloomfield, G. G. Wallace, I. Diez-Perez and M. L. Coote, *Nature*, 2016, **531**, 88–91.
36 Y.-H. Wang, H. Huang, Z. Yu, J.-F. Zheng, Y. Shao, X.-S. Zhou, J.-Z. Chen and J.-F. Li, *J. Mater. Chem. C*, 2020, **8**, 6826–6831.
37 A. I. Yanson, G. R. Bollinger, H. E. van den Brom, N. Agraït and J. M. van Ruitenbeek, *Nature*, 1998, **395**, 783–785.
38 W. Hong, H. Valkenier, G. Mészáros, D. Z. Manrique, A. Mishchenko, A. Putz, P. M. García, C. J. Lambert, J. C. Hummelen and T. Wandlowski, *Beilstein J. Nanotechnol.*, 2011, **2**, 699–713.
39 Y. Song and T. Lee, *J. Mater. Chem. C*, 2017, **5**, 7123–7141.
40 C. Tang, L. Chen, L. Zhang, Z. Chen, G. Li, Z. Yan, L. Lin, J. Liu, L. Huang, Y. Ye, Y. Hua, J. Shi, H. Xia and W. Hong, *Angew. Chem., Int. Ed.*, 2019, **58**, 10601–10605.
41 O. Adak, E. Rosenthal, J. Meisner, E. F. Andrade, A. N. Pasupathy, C. Nuckolls, M. S. Hybertsen and L. Venkataraman, *Nano Lett.*, 2015, **15**, 4143–4149.
42 Y. Chen, H.-C. Wang, Y. Tang, Y. Zhou, L. Huang, J. Cao, C. Tang, M. Zhang, J. Shi, J. Liu, X. Ren, Y.-X. Xu and W. Hong, *Chem. Commun.*, 2021, **57**, 1935–1938.
43 Z. Chen, L. Chen, G. Li, Y. Chen, C. Tang, L. Zhang, J. Liu, L. Chen, Y. Yang, J. Shi, J. Liu, H. Xia and W. Hong, *Cell Rep. Phys. Sci.*, 2021, **2**, 100329.
44 Y. Tang, Y. Zhou, D. Zhou, Y. Chen, Z. Xiao, J. Shi, J. Liu and W. Hong, *J. Am. Chem. Soc.*, 2020, **142**, 19101–19109.
45 K. S. Thygesen and K. W. Jacobsen, *Chem. Phys.*, 2005, **319**, 111–125.
46 B. Capozzi, J. Xia, O. Adak, E. J. Dell, Z.-F. Liu, J. C. Taylor, J. B. Neaton, L. M. Campos and L. Venkataraman, *Nat. Nanotechnol.*, 2015, **10**, 522–527.

47 M. H. Garner, H. Li, Y. Chen, T. A. Su, Z. Shangguan, D. W. Paley, T. Liu, F. Ng, H. Li, S. Xiao, C. Nuckolls, L. Venkataraman and G. C. Solomon, *Nature*, 2018, **558**, 415–419.
48 G. C. Solomon, C. Herrmann, T. Hansen, V. Mujica and M. A. Ratner, *Nat. Chem.*, 2010, **2**, 223–228.
49 M. Brandbyge, J.-L. Mozos, P. Ordejón, J. Taylor and K. Stokbro, *Phys. Rev. B: Condens. Matter Mater. Phys.*, 2002, **65**, 165401.